Off-resonance intracavity up-conversion pumping architecture enabling multi-watt operation of a 2.3-μm Tm:YLF laser

Matthieu Glasset, Hippolyte Dupont, Lauren Guillemot, Pavel Loiko, Patrice Camy, Patrick Georges, Frédéric Druon

Research Article | Vol. 33, No. 5 / 10 Mar 2025 / Optics Express 10715
Optics EXPRESS

Off-resonance intracavity up-conversion pumping architecture enabling multi-watt operation of a 2.3-µm Tm:YLF laser

MATTHIEU GLASSET,[1] HIPPOLYTE DUPONT,[1] LAUREN GUILLEMOT,[2] PAVEL LOIKO,[2] PATRICE CAMY,[2] PATRICK GEORGES,[1] AND FRÉDÉRIC DRUON[1,*]

[1] *Université Paris-Saclay, Institut d'Optique Graduate School, CNRS, Laboratoire Charles Fabry, 91127 Palaiseau, France*
[2] *Centre de Recherche sur les Ions, les Matériaux et la Photonique (CIMAP), UMR 6252 CEA-CNRS-ENSICAEN, Université de Caen, 6 Boulevard Maréchal Juin, 14050 Caen Cedex 4, France*
[*] *frederic.druon@institutoptique.fr*

Abstract: We present an intra-cavity upconversion pumping scheme for Thulium lasers operating on the $^3H_4 \rightarrow {}^3H_5$ transition. It is based on detuning the pump wavelength from the resonance of excited-state absorption, $^3F_4 \rightarrow {}^3F_{2,3}$, around 1 µm. This scheme is validated using a Tm:$LiYF_4$-based laser. The pump source consists of a diode-pumped Nd:YVO_4 laser emitting at 1.064 µm. This architecture permits for power scaling of 2.3-µm Tm-lasers. An output power of 2.7 W is generated in the continuous-wave regime for 62.3 W of intracavity pump power at 1.064 µm corresponding to 21 W of primary laser-diode power, making this kind of pumping competitive in terms of power, laser gain and efficiency with direct diode pumping at 0.78 µm. We also describe the heat management in this double-cavity laser benefiting from the intra-cavity pumping architecture allowing to share the thermal load between two gain crystals. The low absorption caused by the non-resonant $^3F_4 \rightarrow {}^3F_{2,3}$ Tm^{3+} transition allows the Nd pump laser to reach higher intracavity power compensating for the low pump absorption efficiency in the Tm-crystal. The proposed off-resonance pumping scheme opens a new paradigm that holds great promise for high-power, high-gain 2.3 µm solid-state lasers based on thulium ions.

1. Introduction

Coherent sources emitting around 2.3 µm find numerous applications, which explains the recent surge of interest for such lasers. Indeed, these sources are ideally placed in the K transmission band of the atmosphere, making them excellent candidates for LIDAR applications [1]. Such lasers are also used to study combustion processes, as well as to perform non-invasive glycemia testing [2]. Different types of sources have been developed around 2.3 µm, using optical parametric oscillators or amplifiers [3], semiconductor lasers [4], or solid-state lasers based on transition-metal or rare-earth ions directly emitting at this wavelength. Indeed, Cr^{2+}:ZnSe and Cr^{2+}:ZnS lasers cover the spectral range around 2.3 µm [5]. Furthermore, thulium (Tm^{3+}) doped materials operating on the $^3H_4 \rightarrow {}^3H_5$ electronic transition can address this wavelength [6,7].

Thulium lasers operating at 2.3 µm present a variety of pumping schemes. To date, pumping from the ground state ($^3H_6$) directly to the upper laser level ($^3H_4$) using commercial Ti:Sapphire lasers tuned to 0.78 µm offered high laser slope efficiencies surpassing the Stokes limit [8,9]. Generation of multi-watt laser output powers using fiber-coupled, spatially multimode 0.78-µm AlGaAs laser diode modules as pump sources was further demonstrated [10–12]. In recent studies, the upconversion pumping schemes also showed promising results [13,14]. After an

#545266 https://doi.org/10.1364/OE.545266
Journal © 2025 Received 18 Oct 2024; revised 22 Dec 2024; accepted 31 Jan 2025; published 3 Mar 2025

Optics EXPRESS

off-resonant ground-state absorption (GSA) relying on a short-wave phonon sideband of the $^3H_6 \rightarrow {}^3H_5$ transition and a non-radiative relaxation (NR) step to populate the intermediate metastable level $^3F_4$ (luminescence lifetime: $\tau_{lum} = 11$ ms for the Tm:LiYF$_4$ crystal (shortly Tm:YLF)), a resonant excited-state absorption (ESA) $^3F_4 \rightarrow {}^3F_{2,3}$ followed by another NR step fills the upper laser level $^3H_4$. Upconversion pumping is further promoted by the cross-relaxation (CR) process for adjacent Tm^{3+} ions, $^3H_4 + {}^3H_6 \rightarrow {}^3F_4 + {}^3F_4$, even although it depopulates the $^3H_4$ level, as at the same time this phonon-assisted process helps to populate the $^3F_4$ metastable level seeding ESA from this manifold, Fig. 1(a).

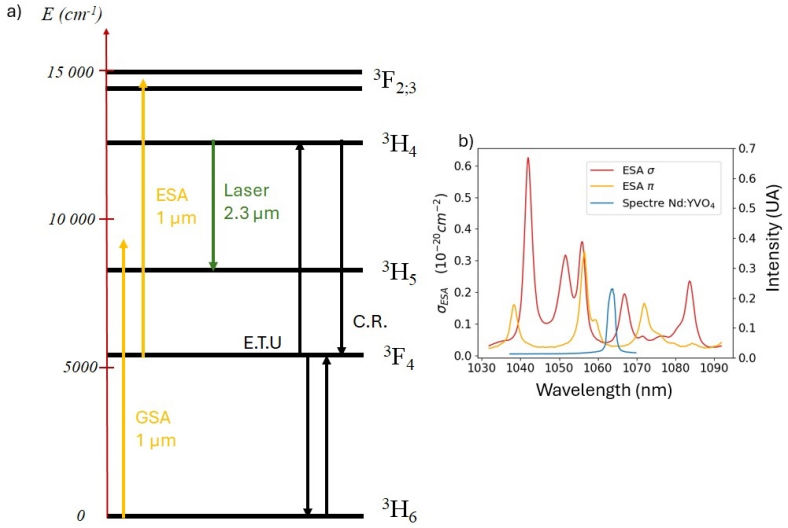

Fig. 1. (a) Energy-level scheme of thulium ions. GSA and ESA: ground- and excited-state absorption, respectively, ETU: energy-transfer upconversion. CR: cross-relaxation. (b) ESA cross-sections for the $^3F_4 \rightarrow {}^3F_{2,3}$ transition of Tm^{3+} ions in LiYF$_4$ for light polarizations σ and π [30]. The output spectrum of the Nd:YVO$_4$ laser is shown for comparison.

Upconversion pumping has been successfully demonstrated in 2.3-µm Tm-lasers based on glass fibers [13] and bulk crystals [14–16] taking the advantages of the well-established technology of 1-µm laser sources, notably, their power scalability and near diffraction-limited output beam quality. One of the key limitations of upconversion pumping schemes stems from the fact that the pump absorption is strongly dependent of the pump intensity, so that high-brightness pumping is required. Moreover, the pump absorption is often limited (measuring about 10% - 40% in single pass [14,15,17]) and it cannot be easily boosted as this would require too long active elements and critically high Tm^{3+} doping levels. Recently, Dupont *et al.* proposed an intracavity pumping architecture to address the low absorption issue intrinsic to upconversion pumping [18].

For the particular case of the Tm:YLF laser crystal which is currently considered as the main candidate for efficient and power-scalable 2.3-µm lasers owing to a combination of its appealing thermo-optic and spectroscopic properties, the main challenge is to identify the pump laser whose emission wavelength correctly matches one of the relatively narrow ESA peaks slightly above 1 µm. Employing a Nd:ASL pump laser emitting at 1.05 µm enabling intracavity upconversion pumping of a Tm:YLF crystal, an output power of 1.81 W at 2.3 µm has been demonstrated for an intracavity pump power of 30 W at 1.05 µm [18] corresponding to a power of the primary pump diode of 42 W at 790 nm. Similar intracavity pumping schemes have also been reported for other laser transitions of rare-earth ions [19–22].

One interesting question to raise concerning the intracavity pumping scheme is its remarkable adaptability with respect to absorption. By absorbing less pump power at ~1 µm, the Tm-crystal

Optics EXPRESS

introduces less losses inside the pumping cavity thereby allowing the intra-cavity power to be higher. This observation motivated us to focus on pump wavelengths detuned not only from the GSA lines, but also from the narrow ESA absorption peaks of Tm^{3+} ions, leveraging the requirements for the choice of the pump laser.

In this work, we report on a proof-of-concept of *off-resonance* intracavity upconversion pumping relying on the well-developed technology of diode-pumped Nd:YVO_4 lasers emitting at 1.064 µm, benefiting from the high efficiency and high gain of these sources. Using an off-resonance pump laser, Fig. 1(b), it is expected that the intrinsic feedback of the double-cavity laser will compensate for the lack of pump absorption by having higher intracavity power favored by the high gain of the Nd:YVO_4 crystal. By combining this high gain with the relatively weak absorption of the Tm-crystal in the case of off-resonance pumping, the intracavity pumping presents a great opportunity to develop a novel approach for high-power, efficient 2.3 µm lasers that are competitive with the direct diode-pumping scheme.

2. Laser setup

The primary pump source consists of a high-power fiber-coupled (numerical aperture, N.A. = 0.22, fiber core diameter: 200 µm) AlGaAs laser diode delivering up to 40 W at 0.8 µm with a spatially multimode output. This laser diode is used to pump a 5 mm-long, 1 at.% Nd:YVO_4 laser crystal. The input face of the Nd-crystal is coated to achieve high transmission (HT) at 0.8 µm and high reflection (HR) at 1.064 nm thus serving as a pump mirror. Another surface of this crystal is antireflection coated for both the pump and laser wavelengths. The Nd-crystal is placed in a V-shaped cavity. The concave folding mirror, placed at 20 cm from the crystal, (radius of curvature: RoC = -300 mm) provides HT at 0.8 µm and HR at 1.064 µm thus removing the residual (non-absorbed) pump. Another cavity arm is terminated by a plane highly reflective mirror with the goal of optimizing the intracavity power at 1.064 µm.

Furthermore, we nest the 2.3 µm V-shaped Tm-laser cavity inside the pumping cavity, as depicted in Fig. 2(a). To realize this, inside the 1.064-µm cavity, we use two dichroic mirrors coated for HT at 1.064 µm and HR at 2.3 µm. One of them is flat, placed at approximately 1 m from the 1.064 µm folding mirror, and acts as a rear mirror, while the other one is concave (RoC = -200 mm), placed at roughly 8 cm from the first one, acting as a folding mirror. The intracavity dichroic mirrors allow for circulation of the 1.064-µm pump radiation through the Tm-crystal. A secondary beam waist for the 1.064-µm laser is created using a pair of antireflection coated intracavity lenses (focal lengths: $f = 80$ mm and 100 mm). The Tm:YLF crystal is placed in this secondary beam waist at normal incidence. The estimated waist size for the 1.064-µm laser mode is 45 µm. The Tm-laser cavity is terminated by a plane output coupler (OC) allowing for extraction of the 2.3-µm radiation. We study multiple ***a***-cut Tm:YLF laser crystals, allowing us to explore a range of Tm^{3+} doping concentrations from 2 at.% to 6 at.% Tm, and different output coupler transmissions ranging from 0.85% to 3.1%. To extend the range of the available effective output coupling rates, we adapt the 2.3-µm laser cavity by allowing multiple bounces on different couplers as shown on the inset in Fig. 2(b). This setup allows oscillations, of both the Nd:YVO_4 and Tm:YLF lasers, in the continuous-wave regime without instabilities.

The stimulated-emission cross-section of Nd^{3+} ions in YVO_4 is $12 \times 10^{-19}\,cm^{-2}$ at 1.064 µm for light polarization π, and due to a strong intrinsic gain anisotropy of the Nd:YVO_4 crystal, the 1.064 µm laser emission has linear polarization being independent of the absorption loss anisotropy of the Tm:YLF crystal. The ESA cross-sections of Tm^{3+} ions in $LiYF_4$ at 1.064 µm amount to $0.08 \times 10^{-20}\,cm^{-2}$ and $0.04 \times 10^{-20}\,cm^{-2}$ for σ and π light polarizations, respectively, see Fig. 1(b). As the pump radiation is linearly polarized, one can choose the pump polarization of the Tm:YLF crystal by simply rotating it at 90°.

Optics EXPRESS

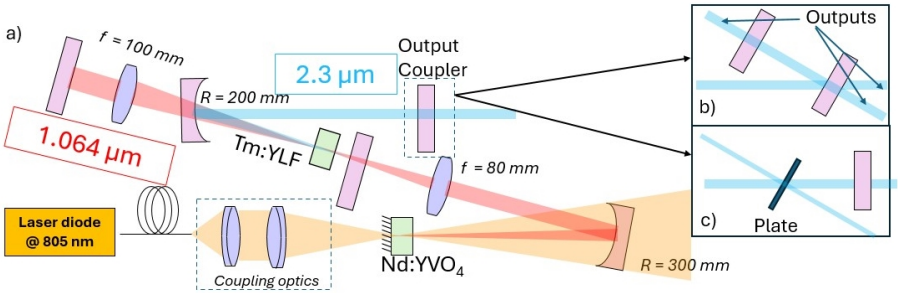

Fig. 2. 2.3-µm Thulium laser based on a Tm:$LiYF_4$ crystal with off-resonance intracavity upconversion pumping by a 1.064-µm diode-pumped Nd:YVO_4 laser: (a) layout of the laser setup; (b,c) optional configurations of the collimated arm of the 2.3-µm laser cavity: (b) adding bounces on different couplers to explore higher output coupling rates; (c) introducing losses via an uncoated plate of sapphire, CaF_2 or germanium to measure the small-signal gain.

We also perform the measurements of small-signal gain for the 2.3-µm Tm-laser. To do so, since the gain is high, the applied output couplers are not sufficient, and an uncoated plate is inserted in the cavity to vary the Fresnel losses by rotating it, as shown in Fig. 2(c).

3. Polarization anisotropy of 1.064-µm upconversion pumping

The initial experiments have been performed using a 1 cm-thick 2 at.% Tm:YLF crystal and a conventional 3.1% output coupler. Since the selected pump wavelength is not in resonance with any of the discrete and narrow ESA peaks of Tm^{3+} ions in $LiYF_4$, it is interesting to figure out what is the effect of the 1.064-µm pump polarization in the Tm-crystal on its 2.3-µm laser performance. Indeed, as shown in Fig. 1(b), the ESA cross-section at 1.064 µm is higher for σ-polarized light. When operating at pump intensities being sufficiently high to enable the photon avalanche process seeding the ESA from the intermediate $^3F_4$ manifold, the measured pump absorption at 1.064 µm in the Tm-crystal is about 5% per pass for σ polarization and 1.8% per pass for π polarization, Fig. 3(a).

We employed a steady-state rate-equation model that accounts for cross-relaxation driving the photon avalanche mechanism to simulate the dependence of single-pass pump absorption on pump power, as shown by the curves in Fig. 3(a). This approach is similar to that described in [18]. The spectroscopic data were taken from [30]. In addition, we measured the round-trip absorption of the 1.064-µm radiation in the Tm:YLF crystal by monitoring the residual pump after the highly reflective mirror with a radius of curvature of -300 mm. Due to its transmission at 1.064 µm being only 0.16%, this measurement unfortunately resulted in a large error. From these data, we extracted the experimental single-pass absorption shown by the points in Fig. 3(a) along with the error bars. Despite a large r.m.s. deviation of the measured data, they reasonably agree with the model, especially at high pump levels, considering also the precision of the ESA spectral measurements by the pump-probe method.

This difference of absorption naturally leads to a difference in the output power at 2.3 µm which is lower for π polarization pumping than that for σ polarization pumping, measuring 0.7 W and 1.67 W, respectively, for a fixed diode pump power of 14.5 W, Fig. 3(c). Given the lower pump absorption, pumping into π polarization leads to a higher intracavity pump power at 1.064 µm as compared to pumping into orthogonal polarization, reaching 120 W (π) versus 55 W (σ) for a fixed diode pump power of 14.5 W, see Fig. 3(d). However, this significant increase of the intracavity pump power does not fully compensate for the lower pump absorption and, as a result,

Optics EXPRESS

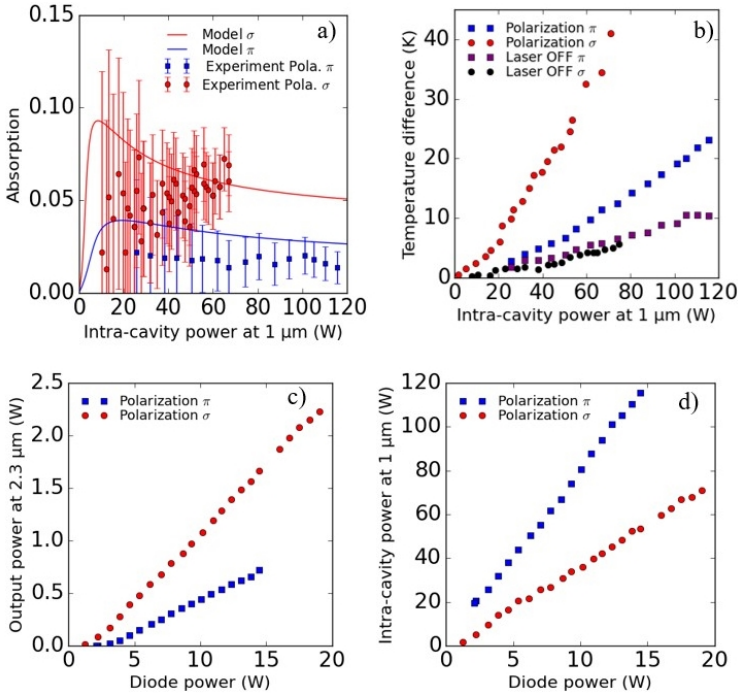

Fig. 3. Effect of the 1.064-μm pump polarization (corresponding to π or σ in the Tm-crystal) on the laser performance for a 1 cm-thick, 2 at.% Tm:YLF crystal: (a) single-pass pump absorption *vs.* intracavity pump power at 1.064 μm: *symbols* – experiment, *curves* – rate-equation modeling; (b) measured temperature difference between the pump spot and the edge of the crystal *vs.* intracavity pump power, with and without laser action at 2.3 μm; (c) output power at 2.3 μm *vs.* laser-diode power; (d) intracavity power at 1.064 μm *vs.* laser-diode power.

the output power at 2.3 μm is lower. For the rest of the study, we will consequently focus on pumping into σ polarization which provided the best results in terms of the power scalability at 2.3 μm.

We also compared thermal effects in the Tm-crystal when pumping into both polarization eigen-states. In the absence of laser emission at 2.3 μm (under non-lasing conditions), the dependences of the measured temperature difference on the intracavity power at 1.064 μm are similar for both pump polarizations, and the temperature rise is relatively low (about 10 K at the maximum intracavity pump power). However, when the 2.3-μm Tm-laser is allowed to operate, the heating is more significant. This effect can be explained by the fact that after emission of a laser photon according to the $^3H_4 \rightarrow {}^3H_5$ transition at 2.3 μm, the $^3H_5 \rightarrow {}^3F_4$ de-excitation is non-radiative and contributes to heat generation. Without laser emission at 2.3 μm, the $^3H_4 \rightarrow {}^3H_5$ path has very low probability, as the corresponding luminescence branching ratio is only 4% [23]. The de-excitation occurs via radiative transitions $^3H_4 \rightarrow {}^3H_6$ and $^3F_4 \rightarrow {}^3H_6$, and the corresponding heat generation is much weaker. Consequently, thermal management of the Tm-crystal is essential for power scaling of 2.3 μm lasers. In the next Section, we will study and try to limit the effect of heating due to the laser emission at 2.3 μm.

Optics EXPRESS

4. Output power and thermal load optimization

We are now going to optimize the laser performance by choosing the optimal output coupling for a 1 cm-thick 2 at.% Tm:YLF crystal, and managing thermal issues. Experimentally, we monitored the output power and the temperature of the crystal surface with a mid-IR thermal camera. We limited the temperature elevation in the Tm-crystal to 100 K to prevent any risk of its thermal fracture. In this case, a temperature difference of 40 K between the central pumping zone and the edge of the crystal is observed.

In this experiment, we show that it is possible to reduce the thermal load by increasing the output coupler transmission at 2.3 µm, see Table 2 summarizing the results. This phenomenon can be explained by the fact that the temperature elevation is primary correlated with the intracavity power at 2.3 µm, Fig. 4(a). To model crystal heating, we assume that the thermal load is uniformly distributed along the entire length of the crystal. This strong assumption is nevertheless justified by the very low absorption of the pump by the crystal and the double-side pumping. In this way, we can model our system with a thermal load uniformly distributed longitudinally and localized within the pumped material volume. In this case, we can express the temperature difference between the crystal center and the periphery using the formula:

$$\Delta T = \frac{P_{abs}}{2\pi\kappa L_{cr}} \times \left[\ln\left(\frac{r_{cr}}{w_p}\right) + 1\right], \tag{1}$$

where P_{abs} is the absorbed power, $\kappa = 5.8$ Wm^{-1}K^{-1} is the thermal conductivity of the material, $L_{cr} = 1$ cm is the crystal length, $r_{cr} = 1.5$ mm is the crystal radius, and $w_p = 45$ µm is the pump waist.

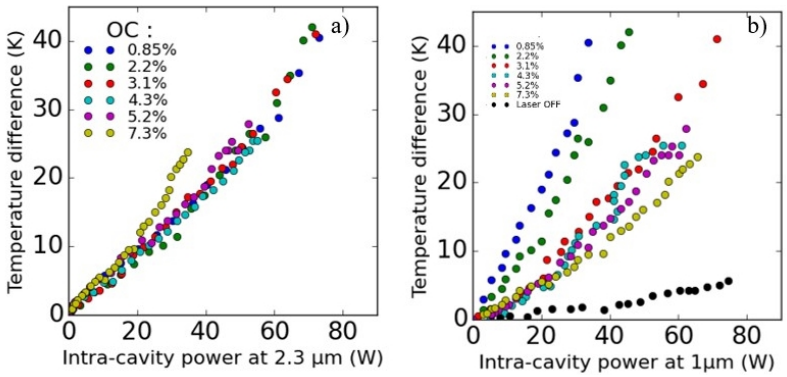

Fig. 4. Temperature difference in the 2 at.% Tm:YLF crystal under intracavity upconversion pumping at 1.064 µm for different output coupler (OC) transmissions: (a) versus the intracavity power at 2.3 µm; (b) versus the intracavity power at 1.064 µm.

Ultimately assuming that all the absorbed pump power is converted into heat, we obtain an upper estimate of the crystal heating. For an intracavity pump power of 42.3 W, this yields a maximum temperature difference ΔT_{max} of 61 K. Table 1 compares the various thermal measurements made, giving an estimate of the fractional heat loading η_h for each coupler at a given diode power.

Therefore, when the output coupling rate increases, the intracavity power at 2.3 µm decreases for the same output at this wavelength. Consequently, it is possible to decrease the heating of the Tm-crystal while maintaining the same output power at 2.3 µm simply by increasing the output coupling (at the expense of an increased laser threshold). To maintain the same laser output at 2.3 µm, one needs to rise the pump power. Since a given intracavity power at 2.3 µm mainly sets

Optics EXPRESS

Table 1. Thermal Load Ratio for Different Output-Coupling Rates in the Intracavity Pumped Thulium Laser

T_{OC} (%)	0.85	2.2	3.1	4.3	5.2	7.3	∅
$P_{in,2.3-\mu m}$ (W)	73	57	41	32	26	18	0
η_h (%)	66.2	42.5	31.9	22.4	20.7	15.6	9.4

Table 2. Output Performance of Upconversion Intracavity Pumped Tm:YLF Laser at 2.3 µm

Doping (at.%)	T_{OC} (%)	Output power at 2.3 µm (W)	Temperature difference ΔT (K)	Laser-diode power P (W)	$\Delta T/P$ (K/W)	Efficiency (%)
2	0.85	0.62	40.5	11.6	3.49	5.4
2	2.2	2.03	42	18.1	2.32	12.8
2	3.1	2.23	41	19	2.15	12.9
2	4.3	2.4	25.5	19.6	1.30	14.4
2	5.2	**2.7**	28	20.4	1.37	**16.8**
2	7.3	2.53	24	21.3	**1.12**	13
2.5	3.1	1.68	20	18.2	1.10	10.6
3	3.1	1.52	26	18.2	1.42	9.6
6	3.1	0.85	50	16	3.13	8

the temperature elevation, increasing the output coupler transmission will permit one to increase the output power (for a given intracavity power) and push forward the temperature limitations. This point is illustrated in Fig. 4(b). For small output coupling rates, we rapidly reach the heating limit of the Tm-crystal, which restricts the pump power at low levels. On the other hand, the use of higher transmissions of the output coupler allows for accessing much higher pump levels. Of course, further increase of the output coupler transmission would involve finding a compromise between an increased laser threshold and deteriorated slope efficiency.

To validate the selection of the optimum output coupler, we also inserted an uncoated CaF_2 plate in the Tm-laser cavity. By rotating it, we could introduce continuously tunable Fresnel losses (with the minimum value corresponding to the Brewster angle). For adequate comparison and to avoid any risk of thermal fracture, we limit the laser diode power to 10 W. By measuring the four Fresnel reflections versus the angle of plate orientation (converted in equivalent output coupler transmission), we find that the best performances are obtained for an output coupling of 6%, as shown in Fig. 5(d). By extrapolating the obtained curve, we estimate that the Tm-laser could operate using much higher output coupler transmission meaning an important small-signal-gain. However, due to the relatively small refractive index of CaF_2, the angle of the plate corresponding to the laser threshold was not accessible without creating diffraction losses at the plate edges. To resolve this problem, we replaced the CaF_2 plate with a germanium one, and we adjusted the pump power to its maximum (for large angles). We measured a round-trip small-signal gain of 2.9 which is, to our best knowledge, the highest value ever reported in the literature for any Tm:YLF laser operating at 2.3 µm. Table 3 overviews the key achievements in the development of 2.3 µm Tm:YLF lasers reported so far.

Optics EXPRESS

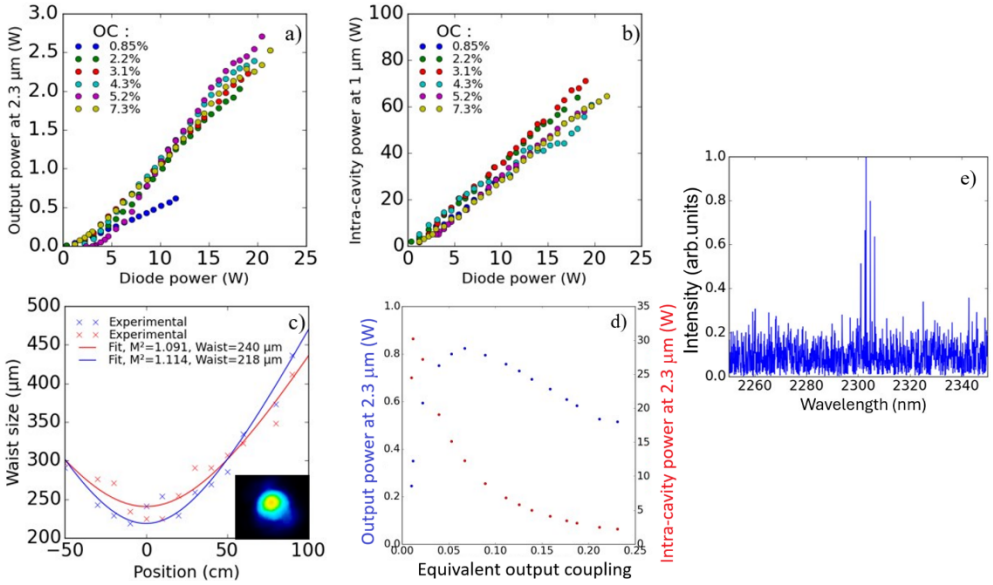

Fig. 5. Optimization of the output performance of an intracavity upconversion pumped 2.3-µm Tm laser employing a 1 cm-thick 2 at.% Tm:YLF crystal: (a) power transfer curves plotted versus laser-diode power at 0.8 µm; (b) intracavity power at 1.064 µm versus laser-diode power; (c) an example M^2 measurement for 2.3-µm laser emission with the corresponding beam profile; (d) total output power at 2.3 µm and the corresponding intracavity power at 2.3 µm for a fixed laser-diode power of 10 W versus the equivalent output coupler transmission (varied via Fresnel reflections on the plate); (e) a typical output spectrum of the 2.3 µm laser.

Table 3. An Overview of Continuous-Wave Tm:YLF Lasers at 2.3 µm Reported so Far

Doping (at.%)	Pump wavelength, Tm crystal (nm)	T_{OC} (%)	Output power at 2.3 µm (W)	Pump power – laser diode (W)	Optical-to-optical efficiency (%)	Ref.
3.5	789 (LD[a])	1.3	1.68	19.1	8.8	[10]
3	790 (LD)	2	**3.1**	34	**9.1**	[28]
1.5	780 (TiSa)	2	0.22	-	11	[31]
1.5	780 (TiSa)	1	0.12	-	12.4	[32]
1.15	685 (LD) and 960 (LD)	1.2	0.5	5 at 685 nm, 20 at 960 nm	2	[33]
3.5	1040 (TiSa)	0.7	0.102		11.7	[14]
3	1055 (Yb-SSL)	1	0.35	30	1.2	[28]
3	1050 (Yb-SSL)	3	0.11	21	0.5	[29]
2.5	1051 (Nd-SSL)	2.5	1.81	42	4.3	[18]
2	1064 (Nd-SSL)	5.2	**2.7**	20.4	**13.2**	This work

[a]Pump sources: LD – laser diode, TiSa – Ti:Sapphire laser, Yb- and Nd-SSL – Ytterbium and Neodymium solid-state laser, respectively.

5. Influence of the Tm doping level

The doping level of the Tm:YLF laser crystal was also varied to enhance understanding and complete the optimization process. We used four different crystals with the doping levels of 2 at.%, 2.5 at.%, 3 at.%, and 6 at.% and respective thicknesses of 10 mm, 8 mm, 8 mm, and 5 mm (all crystals were ***a***-cut).

Optics EXPRESS

First, we observe that for the doping levels above 3 at.%, laser oscillations at 1.9 µm on the $^3F_4 \rightarrow {}^3H_6$ transition could be achieved. Indeed, as one can observe in Fig. 6(b) representing the 2.3-µm laser performance with and without cascade laser operation (*i.e.*, with and without colasing at 1.9 µm [24]), the cascade laser regime is obtained at the expense of the 2.3 µm laser. Consequently, it is better to insert in the cavity a plane mirror coated for high transmission at 1.9 µm to suppress the cascade laser operation. The 1.9 µm emission sinks some of the population of the metastable $^3F_4$ level, thus reducing the exited-state absorption at 1.064 µm from this level and consequently deteriorating the efficiency of the 2.3 µm laser.

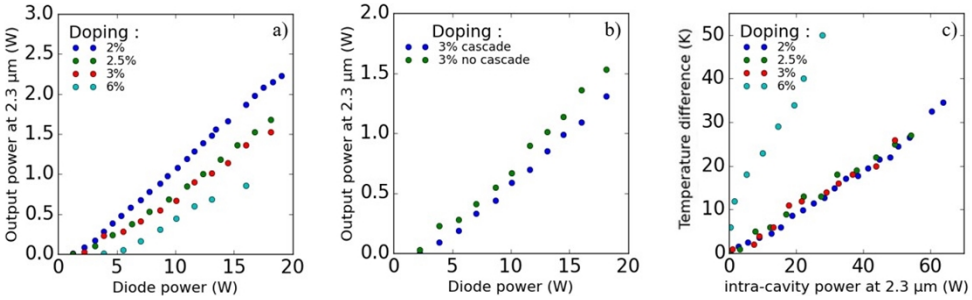

Fig. 6. Effect of the Tm doping level on the output performance and heating of an intracavity upconversion pumped Tm:YLF laser: (a,b) power transfer curves plotted versus laser-diode power: (a) effect of the Tm doping level; (b) effect of the cascade laser operation at 1.9 µm and 2.3 µm on the output performance, 3 at.% Tm-doped crystal; (c) temperature difference between the central pumping zone in the crystal and its edge versus laser-diode power. Output coupling: 3.1%.

The laser performance at 2.3 µm for different active elements was then compared without cascade laser emission, as shown in Fig. 6(a). The 2 at.% Tm-doped crystal provided the best results in terms of slope efficiency and output power. This trend can be easily explained by the dependence of the rate of energy-transfer processes between the active ions on the doping level. By increasing the doping level, we reduce the distances between neighboring ions inside the matrix and, as a main consequence for Tm^{3+} ions, the cross-relaxation effect becomes more significant. In our case, the cross-relaxation process empties the upper level of the laser transition $^3H_4 \rightarrow {}^3H_5$, thus reducing the gain at 2.3 µm.

The deteriorated performance of heavily doped crystals can be partially assigned to more severe thermal issues. We monitored the heating of each crystal during the experiment to reveal the effect of Tm doping on the temperature elevation. We observe that on increasing the doping level, the heating of the crystal substantially increases. In particular, for the 6 at.% Tm-doped crystal, the temperature difference is as high as 50 K for 15 W of laser-diode power, see Fig. 6(c). More generally, for the same intracavity power, the higher the doping level of the crystal, the greater the temperature difference. This phenomenon can be explained by the drop of thermal conductivity of the crystal with rare-earth doping [25–27]. In conclusion, increasing the doping level tends to reduce the performances due to both the cross-relaxation (self-quenching) effect and thermal issues.

6. Conclusion

In conclusion, our study demonstrates a record-high output power at 2.3 µm for any Tm:YLF laser, using an off-resonance intracavity upconversion pumping scheme, achieving 2.7 W at 2.3 µm for 20.5 W of laser-diode power. Indeed, even although the pump absorption of the Tm-crystal at 1.064 µm was only around 5%, it was largely compensated by the intracavity pumping architecture and the use of a high-gain and efficient Nd:YVO_4 laser crystal. By monitoring the temperature

Optics EXPRESS

of the Tm:YLF crystal, we showed that the crystal heating is mainly caused by the 2.3 µm intracavity power. The intracavity pumping scheme allowed us to split the overall thermal load between the Nd:YVO_4 and Tm:YLF crystals which was beneficial for power scaling. Moreover, by optimizing the output coupler transmission, it was possible to operate the laser at higher pump powers avoiding the risk of crystal fracture. After examining the effect of pump polarization on the 2.3-µm laser performance, we conclude that further decreasing absorption would not benefit laser performance. Finally, by studying different doping levels for the Tm:YLF crystal, we showed that lower doping seems more adapted for power scalable laser operation. Moreover, with Tm doping above 3 at.%, even when an upconversion pumping scheme is used, which is conceptually unfavorable for cascade laser operation, a detrimental 1.9 µm laser emission can be observed at the expense of the 2.3 µm laser emission. Finally, we demonstrate that higher doping concentrations also tend to increase the thermal issues in the laser crystal.

Funding. Agence Nationale de la Recherche (19-CE08-0028).

Disclosures. The authors declare no conflicts of interest.

Data availability. Data underlying the results presented in this paper are not publicly available at this time but may be obtained from the authors upon reasonable request.

References

1. G. G. Taylor, D. Morozov, N. R. Gemmell, *et al.*, "Photon counting LIDAR at 2.3 µm wavelength with superconducting nanowires," Opt. Express **27**(26), 38147–38158 (2019).
2. F. J. McAleavey, J. O'Gorman, J. F. Donegan, *et al.*, "Narrow linewidth, tunable Tm^{3+}-doped fluoride fiber laser for optical-based hydrocarbon gas sensing," IEEE J. Sel. Top. Quantum Electron. **3**(4), 1103–1111 (1997).
3. V. Petrov, "Frequency down-conversion of solid-state laser sources to the mid-infrared spectral range using non-oxide nonlinear crystals," Progr. Quantum Electron. **42**, 1–106 (2015).
4. A. Salhi, Y. Rouillard, A. Pérona, *et al.*, "Low-threshold GaInAsSb/AlGaAsSb quantum well laser diodes emitting near 2.3 µm," Semicond. Sci. Technol. **19**(2), 260–262 (2004).
5. I. Moskalev, S. Mirov, M. Mirov, *et al.*, "Ultrafast middle-IR lasers and amplifiers based on polycrystalline Cr:ZnS and Cr:ZnSe," Opt. Mater. Express **7**(7), 2636–2650 (2017).
6. J. Caird, L. DeShazer, and J. Nella, "Characteristics of room-temperature 2.3-µm laser emission from Tm^{3+} in YAG and $YAlO_3$," IEEE J. Quantum Electron. **11**(11), 874–881 (1975).
7. L. Guillemot, P. Loiko, R. Soulard, *et al.*, "Close look on cubic Tm:KY_3F_{10} crystal for highly efficient lasing on the $^3H_4 \rightarrow {}^3H_5$ transition," Opt. Express **28**(3), 3451–3463 (2020).
8. P. Loiko, R. Soulard, L. Guillemot, *et al.*, "Efficient Tm:$LiYF_4$ lasers at ~2.3 µm: Effect of energy-transfer upconversion," IEEE J. Quantum Electron. **55**(6), 1–12 (2019).
9. P. Loiko, E. Kifle, L. Guillemot, *et al.*, "Highly efficient 2.3 µm thulium lasers based on a high-phonon-energy crystal: evidence of vibronic-assisted emissions," J. Opt. Soc. Am. B **38**(2), 482–495 (2021).
10. E. Kifle, P. Loiko, L. Guillemot, *et al.*, "Watt-level diode-pumped thulium lasers around 2.3 µm," Appl. Opt. **59**(25), 7530–7539 (2020).
11. X. Yu, K. Eremeev, Z. Pan, *et al.*, "Six-watt diode-pumped Tm:$GdVO_4$ laser at 2.29 µm," Opt. Lett. **48**(24), 6404–6407 (2023).
12. X. Yu, F. Zha, Z. Pan, *et al.*, "Diode-pumped Tm:YAP laser operating at 2.3 µm with enhanced performance through cascade lasing," Opt. Express **32**(3), 3461–3469 (2024).
13. A. Tyazhev, F. Starecki, S. Cozic, *et al.*, "Watt-level efficient 2.3 µm thulium fluoride fiber laser," Opt. Lett. **45**(20), 5788–5791 (2020).
14. L. Guillemot, P. Loiko, R. Soulard, *et al.*, "Thulium laser at ~2.3 µm based on upconversion pumping," Opt. Lett. **44**(16), 4071–4074 (2019).
15. A. Tyazhev, P. Loiko, L. Guillemot, *et al.*, "Excited-state absorption and upconversion pumping of Tm^{3+}-doped potassium lutetium double tungstate," Opt. Express **31**(9), 14808–14820 (2023).
16. A. Tyazhev, J. E. Bae, M. Gaulke, *et al.*, "Upconversion-pumped femtosecond thulium laser at 2309 nm mode-locked by a GaSb-based SESAM," Opt. Express **32**(9), 15093–15105 (2024).
17. Y. Morova, M. Tonelli, V. Petrov, *et al.*, "Upconversion pumping of a 2.3 µm Tm^{3+}:KY_3F_{10} laser with a 1064 nm ytterbium fiber laser," Opt. Lett. **45**(4), 931–934 (2020).
18. H. Dupont, T. Lenfant, L. Guillemot, *et al.*, "High-power 2.3 µm Tm:YLF laser with intracavity upconversion pumping by a Nd:ASL laser at 1051 nm," Opt. Lett. **49**(8), 2093–2096 (2024).
19. S. So, J. I. Mackenzie, D. P. Shepherd, *et al.*, "Intra-cavity side-pumped Ho:YAG laser," Opt. Express **14**(22), 10481–10487 (2006).
20. R. C. Stoneman and L. Esterowitz, "Intracavity-pumped 2.09-µm Ho:YAG laser," Opt. Lett. **17**(10), 736–738 (1992).
21. E. Herault, F. Balembois, P. Georges, *et al.*, "1064 nm Nd:YVO_4 laser intracavity pumped at 912 nm and sum-frequency mixing for an emission at 491 nm," Opt. Lett. **33**(14), 1632–1634 (2008).

Optics EXPRESS

22. J. M. Serres, P. A. Loiko, X. Mateos, *et al.*, "Ho:KLuW microchip laser intracavity-pumped by a diode-pumped Tm:KLuW laser," Appl. Phys. B **120**(1), 123–128 (2015).
23. B. M. Walsh, N. P. Barnes, and B. Di Bartolo, "Branching ratios, cross sections, and radiative lifetime of rare earth ions in solids: Application to Tm^{3+} and Ho^{3+} ions in $LiYF_4$," J. Appl. Phys. **83**(5), 2772–2787 (1998).
24. H. Dupont, P. Loiko, A. Tyazhev, *et al.*, "Tm:CALGO lasers at 2.32 µm: cascade lasing and upconversion pumping," Opt. Express **31**(12), 18751–18764 (2023).
25. R. Gaumé, B. Viana, D. Vivien, *et al.*, "A simple model for the prediction of thermal conductivity in pure and doped in saluting crystals," Appl. Phys. Lett. **83**(7), 1355–1357 (2003).
26. R. Gaume, "A crystal chemistry approach for high-power ytterbium doped solid-state lasers. Diffusion-bonded crystals and new crystalline hosts," PhD thesis (Chimie ParisTech, 2002).
27. Y. Sato, J. Akiyama, and T. Taira, "Effects of rare-earth doping on thermal conductivity in $Y_3Al_5O_{12}$ crystals," Opt. Mater. **31**(5), 720–724 (2009).
28. X. Zhou, J. Li, S. Huang, *et al.*, "High-efficiency 2.3 µm Tm:YLF laser based on 0.79 µm and 1.05 µm dual-wavelength pumping scheme," Opt. Express **32**(19), 33262–33270 (2024).
29. H. Dupont, L. Guillemot, P. Loiko, *et al.*, "Dual-wavelength-pumping of mid-infrared Tm:YLF laser at 2.3 µm: demonstration of pump seeding and recycling processes," Opt. Express **30**(18), 32141–32150 (2022).
30. L. Guillemot, "Etude de la transition $^3H_4 \rightarrow {}^3H_5$ de l'ion Tm^{3+} pour une émission laser moyen infrarouge (entre 2 et 3 µm),", PhD thesis (Université de Caen Normandie, 2021).
31. J. F. Pinto, L. Esterowitz, and G. H. Rosenblatt, "Tm^{3+}:YLF laser continuously tunable between 2.20 and 2.46 µm," Opt. Lett. **19**(12), 883–885 (1994).
32. I. Yorulmaz and A. Sennaroglu, "Low-threshold diode-pumped 2.3-µm Tm^{3+}:YLF lasers," IEEE J. Sel. Top. Quantum Electron. **24**(5), 1–7 (2018).
33. P. S. de Matos, N. U. Wetter, L. Gomes, *et al.*, "A high power 2.3 µm Yb:Tm:YLF laser diode-pumped simultaneously at 685 and 960 nm," J. Opt. A: Pure Appl. Opt. **10**(10), 104009 (2008).